HHS Public Access

Author manuscript

Nature. Author manuscript; available in PMC 2015 June 17.

Published in final edited form as:

Nature. 2013 August 8; 500(7461): 237–241. doi:10.1038/nature12445.

Pyrimidine homeostasis is accomplished by directed overflow metabolism

Marshall Louis Reaves[1,2], **Brian D. Young**[1,2], **Aaron M. Hosios**[1,2], **Yi-Fan Xu**[1,3], and **Joshua D. Rabinowitz**[1,2,3]

[1]Lewis-Sigler Institute for Integrative Genomics, Princeton University, Princeton, New Jersey 08544, USA

[2]Department of Molecular Biology, Princeton University, Princeton, New Jersey 08544, USA

[3]Department of Chemistry, Princeton University, Princeton, New Jersey 08544, USA

Abstract

Cellular metabolism converts available nutrients into usable energy and biomass precursors. The process is regulated to facilitate efficient nutrient use and metabolic homeostasis. Feedback inhibition of the first committed step of a pathway by its final product is a classical means of controlling biosynthesis[1–4]. In a canonical example, the first committed enzyme in the pyrimidine pathway in *Escherichia coli* is allosterically inhibited by cytidine triphosphate[1,4,5]. The physiological consequences of disrupting this regulation, however, have not been previously explored. Here we identify an alternative regulatory strategy that enables precise control of pyrimidine pathway end-product levels, even in the presence of dysregulated biosynthetic flux. The mechanism involves cooperative feedback regulation of the near-terminal pathway enzyme uridine monophosphate kinase[6]. Such feedback leads to build-up of the pathway intermediate uridine monophosphate, which is in turn degraded by a conserved phosphatase, here termed UmpH, with previously unknown physiological function[7,8]. Such directed overflow metabolism allows homeostasis of uridine triphosphate and cytidine triphosphate levels at the expense of uracil excretion and slower growth during energy limitation. Disruption of the directed overflow regulatory mechanism impairs growth in pyrimidine-rich environments. Thus, pyrimidine homeostasis involves dual regulatory strategies, with classical feedback inhibition enhancing metabolic efficiency and directed overflow metabolism ensuring end-product homeostasis.

Correspondence and requests for materials should be addressed to J.D.R. (joshr@genomics.princeton.edu).

Full Methods and any associated references are available in the online version of the paper.

Supplementary Information is available in the online version of the paper.

Author Contributions M.L.R., A.M.H., B.D.Y., Y.-F.X. and J.D.R. designed experiments and analyses. B.D.Y. generated feedback-dysregulated strains and performed experiments on regulation of the de novo pathway. A.M.H. performed competitions, microarrays and metabolite quantification. M.L.R. generated overflow and cooperativity mutants and measured their metabolites and growth. M.L.R. and J.D.R. wrote the paper with input from all authors.

Author Information The authors declare no competing financial interests. Readers are welcome to comment on the online version of the paper.

The metabolic network of *E. coli* consists of approximately 1,000 metabolites connected by around 2,000 enzyme-catalysed reactions[9]. Control of metabolite concentrations and fluxes occurs through the regulation of enzyme concentrations, activities and substrate occupancies. Metabolic control analysis provides a systematic framework for investigating the impact of particular enzymes on cellular metabolic activities[10–13]. Studies modulating the concentrations of enzymes suggest that control of metabolic flux is frequently distributed across multiple enzymes, with demand for end product often having a key role in controlling biosynthetic fluxes[2,14–16].

Consistent with distributed flux control, *de novo* pyrimidine biosynthesis has been reported to be regulated both at the first committed pathway step, catalysed by aspartate transcarbamoylase (ATCase), and the previous step, catalysed by carbamoyl phosphate synthetase (CPSase), which also feeds arginine biosynthesis. The *E. coli* ATCase enzyme complex, which consists of six catalytic and six regulatory subunits, is subject to feedback inhibition by the pyrimidine end products uridine triphosphate (UTP) and more strongly cytidine triphosphate (CTP), and is activated by ATP[1,5,17–19]. Its allosteric regulation provided one of the first examples of feedback inhibition[3,4]. CPSase is feedback inhibited by the pyrimidine intermediate uridine monophosphate (UMP)[20].

To explore the physiological relevance of ATCase and CPSase allostery, we created strains dysregulated for feedback control of ATCase (Δ*pyrI*), CPSase (*carB** (*carB*(*S948F*))[21]) or both (Δ*pyrI carB**) (Fig. 1a). We then analysed the metabolite concentrations in these strains by liquid chromatography–mass spectrometry (LC–MS)-based metabolomics. We anticipated that such strains would have increased levels of pyrimidine nucleotide triphosphates (NTPs)[2,11,16], the pathway's terminal products; however, UTP and CTP levels were steady in the absence of feedback control. Instead, the only notable change we observed was markedly increased uracil levels (Fig. 1b–d). To understand the robustness of this pathway, we also conducted transcriptome analysis. Rather than compensatory downregulation of pyrimidine biosynthetic genesin the Δ*pyrI carB** strain, we observed modest upregulation. In addition, we observed enhanced expression of genes involved in arginine synthesis (which also requires CPSase) and of the Rut pathway (a recently discovered uracil-degradation pathway that is induced by uracil) (Supplementary Fig. 1)[22].

To assess the homeostatic capacity of pyrimidine metabolism in response to pyrimidine intermediate addition, we switched *E. coli* grown on minimal media to media containing orotate or uracil. Such pyrimidine upshift was sufficient to activate feedback inhibition of pyrimidine synthesis in the wild type, as evidenced by reduced *N*-carbamoyl-aspartate and dihydroorotate concentrations within 5 min; this decrease did not occur in the Δ*pyrI carB** strain (Fig. 1e and Supplementary Fig. 2). In addition, pyrimidine upshift led to markedly increased uracil, and in the case of orotate addition, also UMP, and these increases were observed in all genetic backgrounds (Fig. 1e). Moreover, in both the presence and absence of feedback control, there were only minor increases in UTP and CTP.

Given the end-product homeostasis in the doubly feedback-dysregulated strain, even upon pyrimidine upshift, we sought to confirm that the Δ*pyrI carB** strain is indeed defective in *de novo* pyrimidine biosynthetic regulation. To this end, we measured the incorporation of

isotopically labelled uracil or orotate into UTP and CTP. Similar to the wild-type strain, the Δ*pyrI carB** strain imported the labelled intermediates and incorporated them into end products. The residual production of unlabelled end products, indicative of persistent *de novo* synthesis, however, was higher in the Δ*pyrI carB** strain (Fig. 1f and Supplementary Fig. 2). This confirms that feedback regulation is functionally impaired.

If the feedback-regulation mechanisms facilitated superior pyrimidine homeostasis, perhaps too subtle to be detected by our LC–MS methods, we expected that the feedback-dysregulated strain would have a growth defect relative to its wild-type parent. The Δ*pyrI carB** strain did not, however, exhibit impaired growth in various nutrient conditions, including rich medium, minimal media, media enriched in nucleotides or amino acids, media limited for nitrogen or phosphate, or periodic switches between these conditions (Fig. 1g). We did, however, detect a modest (~10%) growth advantage for the wild-type strain under anoxic conditions and in the presence of the uncoupler 2,4-dinitrophenol.

Slower growth only during energy limitation suggests that the feedback-dysregulated strain engages in a chronic, energy-wasting process. Given the observed uracil excretion, a likely candidate for this inefficient processis the degradation of UMP to uracil. Indeed, orotate addition results in both higher UMP and higher uracil (Fig. 1e), and when the orotate is ^{15}N-labelled, the extent of uracil isotope labelling mimics that of UMP (Supplementary Fig. 3). To elucidate the route from UMP to uracil, we knocked out the genes known to catalyse the interconversion of UMP, uridine and uracil[17]: *udk* (uridine + GTP → UMP + GDP), *upp* (uridine + PRPP R UMP → pyrophosphate (PP_i)) and *udp* (uridine + inorganic phosphate (P_i) → ribose-1-P + uracil). Only the *udp* knockout reduced uracil accumulation, decreasing it to 17% of the level normally found in the feedback-dysregulated background (Fig. 2b). We were able to eliminate uracil production more fully (to 6%) by double deletion of *udp* and the cytosine deaminase *codA*. Following orotate addition, this double-deletion mutant feedback-dysregulated strain accumulates uridine instead of uracil (Fig. 2c and Supplementary Fig. 4).

There is no enzyme with a well-described physiological function of UMP degradation to uridine. This reflects the lack of a straightforward genetic screen for such enzymes. Although often annotated as reversible, the Udk and Upp reactions are thermodynamically unfavourable for the degradation of UMP (both ΔG_{Udk} and ΔG_{Uppc} = +22kJ mol^{-1} based on $\Delta G°_{Udk}$ = +19.5 kJ mol^{-1} and $\Delta G°_{Upp}$ = +20 kJ mol^{-1} and [GTP] = 4.9 mM, [GDP] = 0.68 mM, [uracil] = 5.5 mM, [uridine] = 0.15 mM, [UMP] = 0.5 mM, [diphosphate] = ~1 mM and [PRPP] = 0.26 mM[23,24]), and indeed, their genetic deletion does not prevent uracil accumulation (Fig. 2b). On the basis of published *in vitro* enzymology and homology[17], we identified ~15 putative UMP phosphatase, hydrolase and nucleotidase genes with unknown physiological functions and screened deletion mutants for uracil levels following orotate addition. We found two genes whose deletion led to lower uracil and higher UMP levels than the wild type (Fig. 2c), indicating a possible role in UMP degradation in conditions of pyrimidine excess. We propose that these genes, *nagD* and *surE*, be renamed *umpH* and *umpG*, respectively, to highlight their newly recognized activities in UMP degradation. UmpH and UmpG belong to the haloacid dehalogenase-like phosphatase family and SurE phosphatase families, respectively, whose members span taxa from bacteria to humans, but

little is known about their physiological importance[7,8,25,26]. We observed that knockout of *umpH*, although not altering pathway end-product levels, impaired growth of *E. coli* upon orotate upshift, with the double deletion showing a stronger phenotype and end-product accumulation (Fig. 2c, d and Supplementary Fig. 4). Thus, UmpH, and to a lesser extent UmpG, function in a UMP-degradation pathway that is required for optimal growth in response to environmental pyrimidine intermediates.

The UmpH and UmpG phosphatases degrade UMP to uridine, which is further degraded by Udp to uracil and ribose-1′-phosphate (cytosine similarly liberated from CMP may be deaminated by CodA to uracil). This overflow pathway dissipates three high-energy phosphate bonds (ATP equivalents) and one NADPH per uracil excreted aerobically, increasing to five ATP and inducing production of ubiquinol under anoxia, which may be problematic (Supplementary Fig. 5). The most straightforward way to control flux through this overflow pathway is through the concentration of its substrate UMP. In all conditions where we observe uracil excretion, we also observe increased intracellular UMP. The normal steady-state UMP concentration (0.052 mM) is below the Michaelis constant (K_m) of UmpH for UMP (0.12 mM), but rises to eight times the K_m under conditions inducing directed overflow metabolism (Fig. 2c). This suggests that UMP accumulation has a central role in triggering the overflow flux.

We sought to identify the molecular underpinnings of UMP accumulation during growth in medium enriched in pyrimidine intermediates. In analysing the regulatory architecture of the pathway, we noticed an additional potential feedback loop near the end of the pathway: UMP kinase (which catalyses the ATP-dependent phosphorylation of UMP to UDP), encoded by *pyrH* (Fig. 3a), is regulated *in vitro* by cooperative (ultrasensitive) inhibition by UTP (Hill-coefficient of 2.8, inhibition constant (K_i) of 154 μM)[6]. This inhibition can be partially overcome by GTP activation[6,27], and thus, like the regulation of ATCase by CTP and ATP, may function to achieve balance between pyrimidine and purine pools. Moreover, regulation at the end of the pathway would have the advantage of minimizing perturbations in UTP and CTP levels in response to alterations in any upstream pathway substrate (for example, not only of the *de novo* pathway, but also uracil, orotate, or their nucleosides).

To test the importance of the cooperative inhibition of UMP kinase by UTP, we created strains expressing mutant forms of UMP kinase with reduced sensitivity to UTP: the N72A mutant has a higher K_i (373 μM for UTP rather than 154 μM), and the D93A has both a higher K_i (332 μM) and less cooperative inhibition (Hill coefficient 1.6 rather than 2.8). Because UMP kinase catalyses an essential reaction, we first transformed wild-type cells with low-copy plasmids (pACYC) carrying a natively expressed *pyrH* allele (*pyrH*^{WT}, N72A or D93A) before knocking out genomic *pyrH* by transduction. We then assayed the growth and metabolic response of these strains to uracil and orotate. Although all three strains grew normally in the absence of pyrimidines and upon uracil addition (Supplementary Fig. 6), orotate addition inhibited growth of all three strains, particularly those with impaired inhibition of UMP kinase by UTP (Fig. 3b). The growth defect of the *pyrH*^{WT} (pACYC::*pyrH*^{WT} Δ*pyrH*) strain was presumably due to mild overexpression of wild-type UMP kinase, as inducible overexpression led to the same response (pAC24N::*pyrH*^{WT} + 0.05 μM isopropyl β-D-1-thiogalactopyranoside (ITPG);

Supplementary Fig. 6). Thus, proper control of UMP kinase protein levels is required for an optimal response to pyrimidine upshift. The cooperative feedback inhibition of UMP kinase by UTP and CTP is also important, as impairment of such regulation led to a profound growth defect upon orotate addition (pACYC::*pyrH(D93A)* Δ*pyrH*, Fig. 3b).

We also detected changes to the nucleotide pools of these *pyrH* mutants in response to orotate addition. In the wild type, orotate addition leads to UMP accumulation without major changes in NTP levels (Fig. 3c). Lack of proper UMP kinase regulation, however, results in increased UTP and decreased ATP. Thus, dysregulated pyrimidine metabolism saps purines, either by increasing their usage (for example, because higher pyrimidine NTPs leads to increased ribosomal RNA biosynthetic rates), decreasing their synthesis (for example, by depleting required substrates), or the combination of these factors.

We designate the general mechanism, whereby feedback inhibition of a downstream pathway step leads to excretion of a pathway intermediate or by-product, directed overflow metabolism (Fig. 4a). Such overflow is triggered by excessive biosynthetic pathway flux and is carried out by a degradation pathway sensitive to levels of an accumulating biosynthetic intermediate. It is analogous to overflow in central carbon metabolism, wherein excessive sugar catabolism (typically via glycolysis) leads to build-up of pyruvate[28], which may be excreted as lactate, ethanol or acetate, depending on the organism. In the case of lactate excretion in humans, inhibition of pyruvate dehydrogenase (by high NADH or inhibitory phosphorylation[29]) has a similar role to the inhibition of UMP kinase in the pyrimidine pathway: it forms a choke point that instead directs the enzyme's normal substrate towards by-product formation and excretion (Fig. 4b). In the case of pyrimidine biosynthesis, the cooperative inhibition of UMP kinase by UTP renders the directed overflow mechanism exquisitely precise in controlling UTP and CTP levels.

Thus, pyrimidine homeostasis involves two strategies for regulation. The canonical feedback architecture contributes to metabolic efficiency by decreasing unnecessary *de novo* flux. Directed overflow metabolism provides end-product homeostasis by diverting excess flux to uracil, thereby ensuring end-product homeostasis in response to altered availability of the full range of pathway substrates and intermediates. These upstream and downstream regulatory mechanisms work in concert to balance speed, efficiency and robustness.

METHODS SUMMARY

E. coli (parent strain NCM3722 (ref. 30)) were prepared for metabolite measurement using a filter culture technique: cell-laden nitrocellulose filters were grown on agarose plates. Pyrimidine upshift was accomplished by transferring filters to plates enriched with indicated supplements. Metabolism was quenched and metabolites concomitantly extracted by placing filters into −20°C solvent (40% methanol, 40% acetonitrile and 20% water with 0.1M formic acid). This solvent mixture reliably extracts nucleotides, nucleosides and bases without their interconversion or degradation. Negative mode LC–MS and LC–MS/MS measurements were performed as previously described[23]. Deletion strains were created by P1 transduction from the Keio deletion collection. Stable strains carrying *carB** were generated by electroporation and lambda Red-mediated recombination of PCR-amplified

S948F into a Δ*carB::kan* strain (where *kan* denotes kanamycin resistance) followed plating and selection for prototrophs on minimal media. Growth was assayed by absorbance at 600nm in a 96-well format using a Biotek Synergy II plate reader. Competitive growth advantage was assessed by co-culture of a marked *lacZ*$^{-}$ (Δ*lacZ::kan*) and an unmarked *lacZ*$^{+}$ strain, determination of relative cell numbers after competitive growth by plating on MacConkey agar containing 1% lactose, and regression analysis of wild type to Δ*pyrI carB** ratios. Unless otherwise indicated, growth media for metabolic studies consisted of Gutnick minimal media with 0.4% glycerol and 10 mM NH_4Cl with triple-washed ultrapure agarose and 0.8 mM orotate as needed.

METHODS

Strains

The wild-type *E. coli* K-12 strain NCM3722 was used in this study as wild type and as parent for all strains in this study because it lacks the *rph*-1 mutation carried by MG1655 that causes pyrimidine pseudo-auxotrophy from reduced expression of orotate phosphoribosyltransferase (*pyrE*)[30]. Single-gene deletion mutants of NCM3722 were generated by P1 transduction[31] of deletion alleles with kanamycin resistance (*kan*) cassettes from the Keio collection[32] and verified using PCR with gene-specific primers. Multiple gene deletions were similarly created serially using the FLP helper plasmid system (pCP20), which was also used to eliminate kanamycin resistance cassettes to produce scarred deletions[33].

The *carB(S948F)* mutant was generated using the lambda-Red recombinase system[33]. A plasmid-borne *S948F* mutant allele of *carB*[21] was amplified from plasmid by PCR (*carB* forward primer, 5′-CGCATAAATCCCTGTTCGAC-3′; *carB* reverse primer, 5′-CCATTCGGCGATTAACAAGT-3′), gel-purified and used to transform a NCM3722 Δ*carB::kan* strain carrying pKD46 and induced with arabinose as described previously[32]. Recombinants were selected on minimal media for pyrimidine and arginine prototrophy and subsequently cured of pKD46. Following screening for loss of all antibiotic resistance (ampicillin and kanamycin), the *carB(S948F)* (*carB**) mutation was confirmed by sequencing.

Strains natively expressing variant *pyrH* alleles in a Δ*pyrH::kan* background were also created using the lambda-Red recombinase system. The pACYC::*pyrH* is the ligation product of XbaI-digested, CAP-treated pACYC184 (all New England Biolabs) with XbaI-digested wild-type *pyrH* generated by PCR from NCM3722 genomic template using primer set (*pyrH* forward primer, 5′-AC<u>TCTAGA</u>CCAA TGCAAAACCCGTCTAT-3′; *pyrH* reverse primer 5′-GA<u>TCTAGA</u>ACTTACG CGGAATCTTACCC-3′) (XbaI sites are underlined). Variant alleles were produced through site-directed mutagenesis (Genewiz) and verified by sequencing. NCM3722 carrying plasmid pACYC::*pyrH* and pKD46 was transformed with a *kan* cassette flanked by *pyrH* homology regions (created by PCR of a Keio collection strain with PAGE-purified primer set (forward, 5′-TTGTAAATTCAGCTAACCCTTGTGGGGCTGCGCTGAATTCCGGGGATCCGTCGACC-3′;reverse, 5′-ACCAAACTGCCTGCAACAATAACGCCTTATAACCAGTGTAGGCTGG

AGCTGCTTCG-3′)) to create a genomic Δ*pyrH::kan* allele. To prevent suppressing mutations, the Δ*pyrH::kan* allele was introduced by P1 transduction to strains carrying *pyrH* alleles on the pACYC plasmid and thereafter strains retained plasmid born resistances in absence of antibiotic.

Strains expressing *pyrH* from IPTG-inducible promoter on the pAC24N were created by transformation with *pAC24N::pyrH* from the Aska collection after removal of green fluorescent protein by NotI digestion and self-ligation[34]. Variant alleles were produced through site-directed mutagenesis (Genewiz) and verified by sequencing. Low-level expression was induced with IPTG as indicated.

Media and bacterial culture

Gutnick glucose minimal medium ('Glucose', Gmin1) refers to a salts mixture[35] with a 0.4% (w/v) glucose carbon source and a 10 mM ammonium chloride nitrogen source unless otherwise stated. 'Glycerol' and 'acetate' refer to the identical Gutnick with 0.4% glycerol or 0.4% sodium acetate, respectively, substituted for glucose. Strains were also grown in media supplemented (+) with one of the following: adenine, arginine, guanosine, hypoxanthine, ornithine, uracil or 2,4-dinitrophenol (all 1 mM). Media with alternative nitrogen sources contained Gutnick salts, 0.4% glycerol and 10 mM total concentration of usable nitrogen. Phosphate-limited MOPS (TekNova) medium was prepared with 0.4% glycerol, 10 mM ammonium chloride and 0.5 mM monobasic potassium phosphate[36]. Anoxia experiments were conducted in Gmin1 media at 37°C inside a chamber containing approximately 90% nitrogen gas, 5% carbon dioxide and 5% hydrogen. Oxygen levels were maintained at 0 p.p.m. and rarely exceeded 100 p.p.m. +/− indicates alternating every 8 h between glycerol minimal media and enriched minimal media as indicated above. 'LB, glucose' indicates cells were alternated between LB and Gmin1 media every 8 h. Difco MacConkey agar (Becton, Dickinson) was prepared according to the manufacturer's instructions with 1% lactose as carbon source.

Metabolite measurements

Cells were cultured and extracted at −20°C 40:40:20 methanol: acetonitrile: water with 0.1 M formic acid[37] using the filter culture method described previously[38]. Low-molecular-weight metabolites were quantitated using both LC–MS[39] and LC–MS/MS[40] at both steady state[23] and following addition of exogenous pyrimidines, including unlabelled and isotopically labelled uracil and orotate. Absolute quantification of uracil and UMP was computed as in ref. 23. LC–MS(/MS) data were analysed using MAVEN software[41]. U-[^{15}N]-tracers (for example, uracil and orotate) were purchased from Cambridge Isotopes Laboratories.

Competition assays

The lacZ^{-} (Δ*lacZ::kan*) derivatives of wild-type and Δ*pyrI carB** strains were prepared as described above. After overnight culture in a 50:50 mix of medium for competition and Gmin1, *lacZ*$^{+}$ and *lacZ*$^{-}$ strains were combined to equal proportions (based on attenuance D_{600}) and were diluted to an OD_{600} of 0.02 in medium for competition to create two paired cultures: wild type *lacZ*$^{-}$ with Δ*pyrI carB* lacZ*$^{+}$ and wild type *lacZ*$^{+}$ with Δ*pyrI carB**

lacZ⁻. Each culture pair was grown at 37°C and generally diluted every 8 h (12 h for media with doubling time over 120 min) into fresh medium to D_{600} of 0.02. Some cultures were diluted into alternating media as indicated above.

The ratio of wild type to Δ*pyrI carB** of the culture was determined by regular plating on MacConkey agar plates with 1% lactose (6–10 replicates). Cultures were diluted to ensure that approximately 100 colonies formed on each plate.

Growth advantage was computed by a linear regression of the ratio of wild-type and mutant strains. The ratio of wild-type to mutant cells in time, t, can be described as $R(t) = R_0 \times 2^{t*(1/W-1/M)}$, where R_0 is the initial ratio, and W and M are the doubling times for the wild type and the mutant, respectively. Performing a linear regression of this equation (R software, http://cran.r-project.org) in logarithmic space allows for computation of the growth advantage.

For 2,4-dinitrophenol, advantage was similarly computed from the growth rate of each strain (*lacZ*+) individually in culture and plotted along the diagonal.

Microarrays

RNA purification, labelling, microarray measurement and data processing were performed as described in ref. 42. In brief, overnights of the wild-type and Δ*pyrI carB** mutant were prepared as above in Gmin2 and grown to mid-exponential phase (D_{600} of 0.4) and then mixed with RNAprotect Bacteria Reagent according to manufacturer's specifications (Qiagen). After 5 min at 25°C, the mixture was pelleted for 10min at 5,000g, and RNA was extracted using the Total RNA Purification kit (Norgen Biotek). Purified total RNA was treated for 30 min using E. coli poly(A) polymerase (New England Biolabs). RNA from the wild-type and Δ*pyrI carB** strains were labelled with Cy5 and Cy3, respectively, using the Two-Colour Low Input Quick Amp Labelling Kit (Agilent). Samples were hybridized to an *E.coli* Gene Expression Microarray (Agilent). Resulting data were analysed using iPAGE[43] and R software.

Growth assays

Absorbance measurements were obtained using a Biotek Synergy II plate reader (Biotek, Winooski, VT)in 96-well formatat 600 nm using clear, flat-bottom plates with two independent biological replicates each consisting of six to eight technical replicates. Cultures included 0.1% Tween-20 to prevent clumping and were sealed with air permeable membrane. To facilitate comparisons, some curves are aligned to D_{600} of 0.03.

Supplementary Material

Refer to Web version on PubMed Central for supplementary material.

Acknowledgments

M.L.R. was supported by an National Science foundation (NSF) Graduate Research Fellowship. J.D.R. was supported by NSF CDI Award CBET-0941143 and CAREER Award MCB-0643859, and DOE-AFOSR Award DE-SC0002077/FA9550-09-1-0580, and an American Heart Association Scientist Development Grant.

References

1. Gerhart JC, Pardee AB. The enzymology of control by feedback inhibition. J Biol Chem. 1962; 237:891–896. [PubMed: 13897943]
2. Savageau MA. Optimal design of feedback-control by inhibition — dynamic considerations. J Mol Evol. 1975; 5:199–222. [PubMed: 1159800]
3. Umbarger HE. Evidence for a negative-feedback mechanism in the biosynthesis of isoleucine. Science. 1956; 123:848–849. [PubMed: 13324101]
4. Pardee AB, Yates RA. Control of pyrimidine biosynthesis in Escherichia coli by a feed-back mechanism. J Biol Chem. 1956; 221:757–770. [PubMed: 13357469]
5. Kantrowitz ER. Allostery and cooperativity in Escherichia coli aspartate transcarbamoylase. Arch Biochem Biophys. 2012; 519:81–90. [PubMed: 22198283]
6. Meyer P, et al. Structural and functional characterization of *Escherichia coli* UMP kinase in complex with its allosteric regulator GTP. J Biol Chem. 2008; 283:36011–36018. [PubMed: 18945668]
7. Kuznetsova E, et al. Genome-wide analysis of substrate specificities of the Escherichia coli haloacid dehalogenase-like phosphatase family. J Biol Chem. 2006; 281:36149–36161. [PubMed: 16990279]
8. Proudfoot M, et al. General enzymatic screens identify three new nucleotidases in *Escherichia coli*. Biochemical characterization of SurE, YfbR, and YjjG. J Biol Chem. 2004; 279:54687–54694. [PubMed: 15489502]
9. Orth JD, et al. A comprehensive genome-scale reconstruction of *Escherichia coli* metabolism—2011. Mol Syst Biol. 2011; 7:535. [PubMed: 21988831]
10. Fell, D. Understanding the Control of Metabolism. Portland Press; 1997.
11. Kacser H, Burns JA, Fell DA. The control of flux. Biochem Soc Trans. 1995; 23:341–366. [PubMed: 7672373]
12. Heinrich R, Rapoport TA. Linear steady-state treatment of enzymatic chains. General properties, control and effector strength. Eur J Biochem. 1974; 42:89–95. [PubMed: 4830198]
13. Crabtree B, Newsholme EA. The derivation and interpretation of control coefficients. Biochem J. 1987; 247:113–120. [PubMed: 3689338]
14. Small JR, Kacser H. Responses of metabolic systems to large changes in enzyme-activities and effectors. 1. The linear treatment of unbranched chains. Eur J Biochem. 1993; 213:613–624. [PubMed: 8477732]
15. Kell DB, Westerhoff HV. Metabolic control theory: its role in microbiology and biotechnology. FEMS Microbiol Rev. 1986; 39:305–320.
16. Hofmeyr JHS, Cornish-Bowden A. Quantitative assessment of regulation in metabolic systems. Eur J Biochem. 1991; 200:223–236. [PubMed: 1879427]
17. Keseler IM, et al. EcoCyc: a comprehensive database of *Escherichia coli* biology. Nucleic Acids Res. 2011; 39:D583–D590. [PubMed: 21097882]
18. Peterson AW, Cockrell GM, Kantrowitz ER. A second allosteric site in *Escherichia coli* aspartate transcarbamoylase. Biochemistry. 2012; 51:4776–4778. [PubMed: 22667327]
19. Wild JR, Loughrey-Chen SJ, Corder TS. In the presence of CTP, UTP becomes an allosteric inhibitor of aspartate transcarbamoylase. Proc Natl Acad Sci USA. 1989; 86:46–50. [PubMed: 2643106]
20. Anderson PM, Meister A. Control of *Escherichia coli* carbamyl phosphate synthetase by purine and pyrimidine nucleotides. Biochemistry. 1966; 5:3164–3169. [PubMed: 5339550]
21. Delannay S, et al. Serine 948 and threonine 1042 are crucial residues for allosteric regulation of *Escherichia coli* carbamoyl phosphate synthetase and illustrate coupling effects of activation and inhibition pathways. J Mol Biol. 1999; 286:1217–1228. [PubMed: 10047492]
22. Loh KD, et al. A previously undescribed pathway for pyrimidine catabolism. Proc Natl Acad Sci USA. 2006; 103:5114–5119. [PubMed: 16540542]
23. Bennett BD, et al. Absolute metabolite concentrations and implied enzyme active site occupancy in *Escherichia coli*. Nature Chem Biol. 2009; 5:593–599. [PubMed: 19561621]

24. Flamholz A, Noor E, Bar-Even A, Milo R. eQuilibrator–the biochemical thermodynamics calculator. Nucleic Acids Res. 2012; 40:D770–D775. [PubMed: 22064852]
25. Bianchi V, Spychala J. Mammalian 5′-nucleotidases. J Biol Chem. 2003; 278:46195–46198. [PubMed: 12947102]
26. Tremblay LW, Dunaway-Mariano D, Allen KN. Structure and activity analyses of *Escherichia coli* K-12 NagD provide insight into the evolution of biochemical function in the haloalkanoic acid dehalogenase superfamily. Biochemistry. 2006; 45:1183–1193. [PubMed: 16430214]
27. Bucurenci N, et al. Mutational analysis of UMP kinase from *Escherichia coli*. J Bacteriol. 1998; 180:473–477. [PubMed: 9457846]
28. Sauer U, Eikmanns BJ. The PEP–pyruvate–oxaloacetate node as the switch point for carbon flux distribution in bacteria. FEMS Microbiol Rev. 2005; 29:765–794. [PubMed: 16102602]
29. Roche TE, Hiromasa Y. Pyruvate dehydrogenase kinase regulatory mechanisms and inhibition in treating diabetes, heart ischemia, and cancer. Cell Mol Life Sci. 2007; 64:830–849. [PubMed: 17310282]
30. Soupene E, et al. Physiological studies of Escherichia coli strain MG1655: growth defects and apparent cross-regulation of gene expression. J Bacteriol. 2003; 185:5611–5626. [PubMed: 12949114]
31. Silhavy, TJ.; Berman, ML.; Enquist, LW. Experiments With Gene Fusions. Cold Spring Harbor Press; 1984.
32. Baba T, et al. Construction of *Escherichia coli* K-12 in-frame, single-gene knockout mutants: the Keio collection. Mol Syst Biol. 2006; 2(2006):0008. [PubMed: 16738554]
33. Datsenko KA, Wanner BL. One-step inactivation of chromosomal genes in *Escherichia coli* K-12 using PCR products. Proc Natl Acad Sci USA. 2000; 97:6640–6645. [PubMed: 10829079]
34. Kitagawa M, et al. Complete set of ORF clones of *Escherichia coli* ASKA library (a complete Set of *E. coli* K-12 ORF archive): unique resources for biological research. DNA Res. 2006; 12:291–299. [PubMed: 16769691]
35. Gutnick D, Calvo JM, Klopotowski T, Ames BN. Compounds which serve as the sole source of carbon or nitrogen for *Salmonella typhimurium* LT-2. J Bacteriol. 1969; 100:215–219. [PubMed: 4898986]
36. Neidhardt FC, Bloch PL, Smith DF. Culture medium for enterobacteria. J Bacteriol. 1974; 119:736–747. [PubMed: 4604283]
37. Rabinowitz JD, Kimball E. Acidic acetonitrile for cellular metabolome extraction from *Escherichia coli*. Anal Chem. 2007; 79:6167–6173. [PubMed: 17630720]
38. Bennett BD, Yuan J, Kimball EH, Rabinowitz JD. Absolute quantitation of intracellular metabolite concentrations by an isotope ratio-based approach. Nature Protocols. 2008; 3:1299–1311.
39. Lu W, et al. Metabolomic analysis via reversed-phase ion-pairing liquid chromatography coupled to a stand alone orbitrap mass spectrometer. Anal Chem. 2010; 82:3212–3221. [PubMed: 20349993]
40. Lu W, Kimball E, Rabinowitz JD. A high-performance liquid chromatography-tandem mass spectrometry method for quantitation of nitrogen-containing intracellular metabolites. J Am Soc Mass Spectrom. 2006; 17:37–50. [PubMed: 16352439]
41. Clasquin MF, Melamud E, Rabinowitz JD. LC-MS data processing with MAVEN: a metabolomic analysis and visualization engine. Curr Protoc Bioinformatics. 2012; 14(14):11. [PubMed: 22389014]
42. Goodarzi H, et al. Regulatory and metabolic rewiring during laboratory evolution of ethanol tolerance in *E coli*. Mol Syst Biol. 2010; 6378
43. Goodarzi H, Elemento O, Tavazoie S. Revealing global regulatory perturbations across human cancers. Mol Cell. 2009; 36:900–911. [PubMed: 20005852]

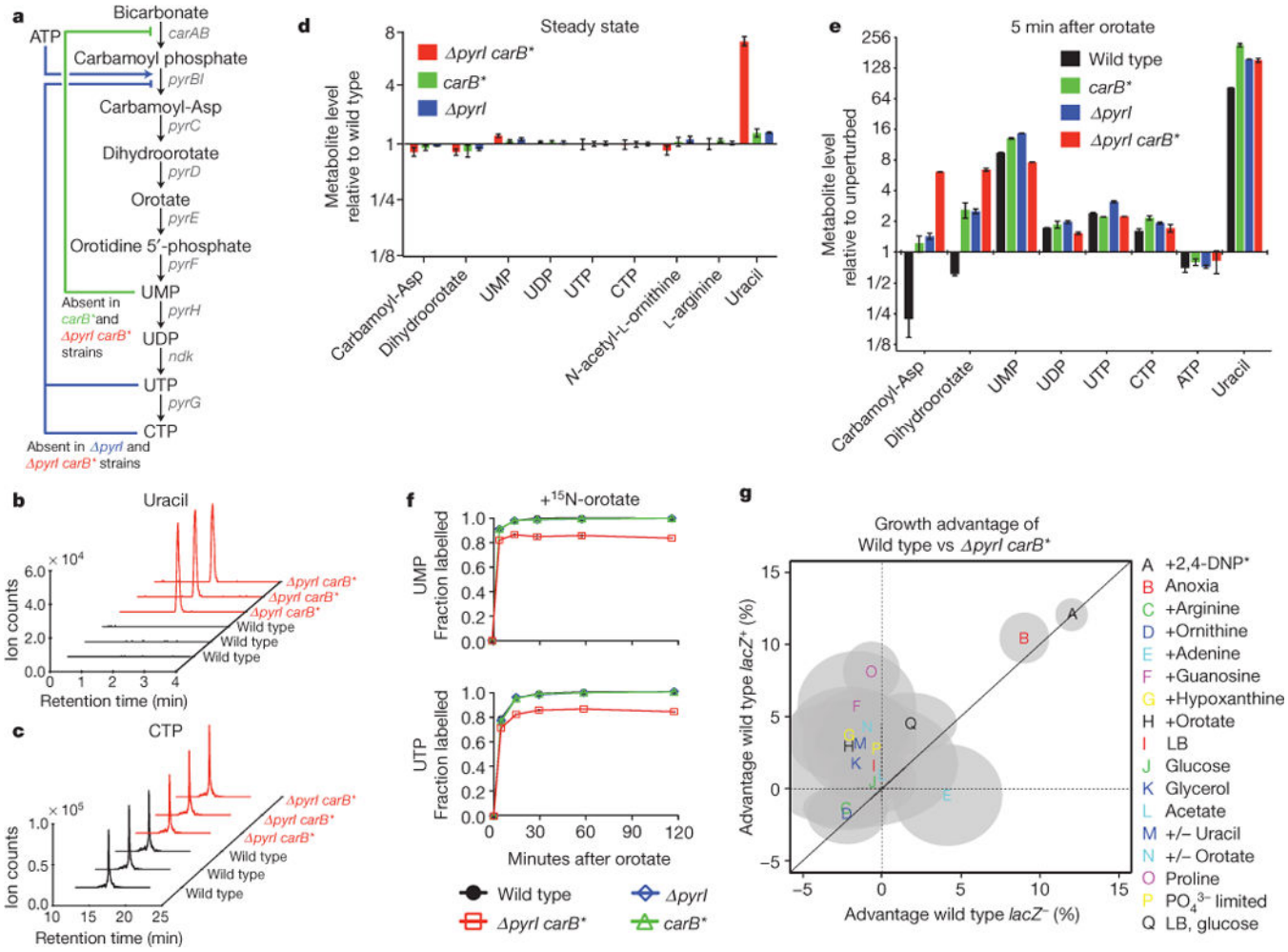

Figure 1. Increased pyrimidine flux triggers overflow to uracil

a, Canonical pyrimidine regulatory schematic. Carbamoyl phosphate is an intermediate in both pyrimidine and arginine synthesis. Carbamoyl aspartate is committed to pyrimidine synthesis. Carbamoyl phosphate synthetase (*carAB*) is feedback inhibited by UMP. Aspartate transcarbamoylase (*pyrBI*) is feedback inhibited by UTP and CTP and activated by ATP. **b, c,** Extracted ion chromatograms showing uracil (**b**) and CTP (**c**) levels in wild-type (black) and feedback-defective (Δ*pyrI carB*;* red) strains. **d,** Metabolite fold changes relative to wild type in Δ*pyrI*, *carB** and Δ*pyrI carB** strains. Error bars denote ± standard error (n = 6). **e,** Metabolite fold changes at 5min after addition of orotate. Fold changes were computed relative to un-supplemented controls. Error bars denote ± standard deviation (n = 2–3). Time course data appear in Supplementary Fig. 2. **f,** Fraction of UMP and UTP derived from endogenous sources and from exogenously added ^{15}N-orotate. Error bars denote ± standard deviation (n = 2). The Δ*pyrI* (blue) and wild-type (black) lines lie under the *carB** (green) line. **g,** Competitive growth advantage of wild-type versus Δ*pyrI carB** appears selectively under energy limitation. Competitions were performed in indicated media with *lacZ*$^{-}$ marker in wild-type and in feedback-dysregulated strain (wild-type *lacZ*$^{+}$) to control for effect of marker on growth. Calculations and experimental details are described in Methods. In brief, media were glucose-ammonia minimal media unless

otherwise indicated. Alternative carbon and nitrogen sources were used in conditions K, L and O. + indicates supplements to the minimal media; +/− indicates alternating supplementation/removal of indicated nutrient every 8 h. Grey ellipses mark 95% confidence interval (n = 6–10).

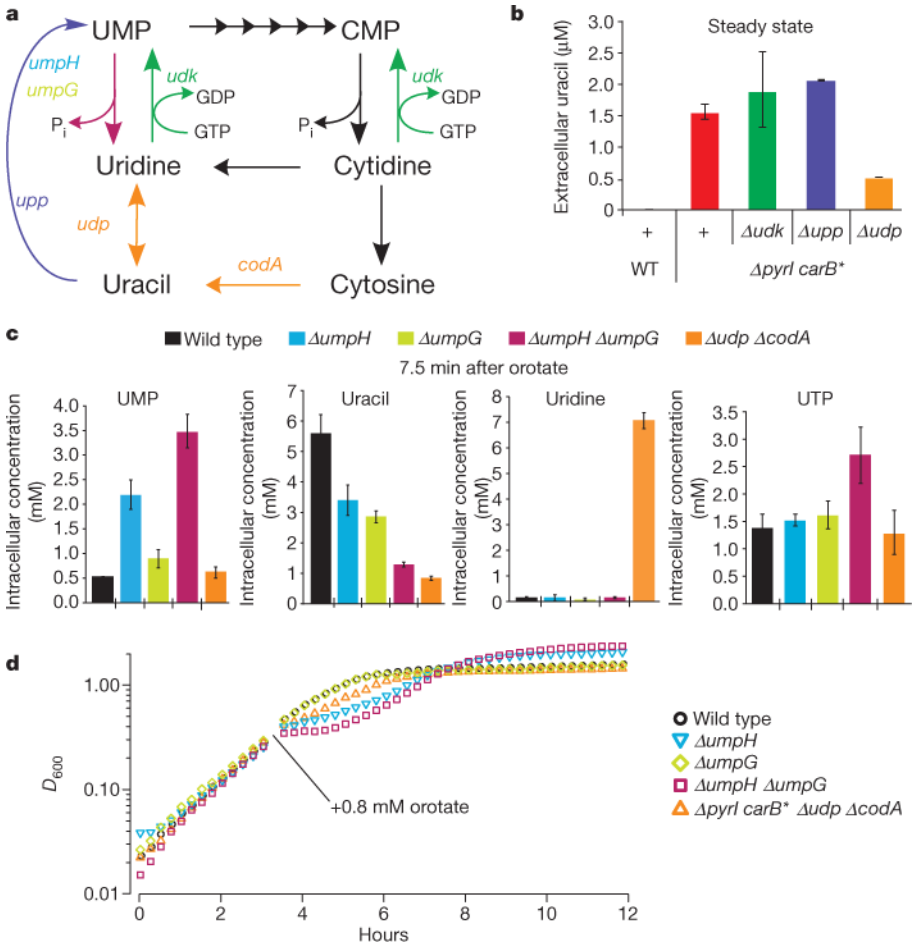

Figure 2. Pyrimidine overflow pathway is initiated by catabolism of UMP by UmpH

a, Pathway schematic. **b,** Uracil excretion does not depend on the canonical pyrimidine interconversion enzymes Udk and Upp, but does require Udp. Excreted uracil accounts for approximately half of total uracil. Error bars mark standard deviation (n = 2–3). c, Uracil is produced by UMP degradation following orotate addition. UMP is degraded to uridine by UmpH (also known as NagD) and UmpG (also known as SurE), and uridine to uracil by Udp. Isotopic tracing from orotate to UMP, uridine and uracil appears in Supplementary Fig. 3. Residual uracil in a Δ*udp* Δ*codA* strain indicates at least one unannotated activity also makes minor contributions to uracil production. End-product levels are not perturbed following orotate addition by deletion of either Δ*umpH* or Δ*umpG* individually, but double deletion leads to increased UTP. Error bars mark ± standard deviation (n =3). **d,** Inability to degrade UMP to uracil causes a growth defect upon orotate addition but increases final culture density (reproducible in two biologically independent experiments each of 6–8 technical replicates). *D*, attenuance.

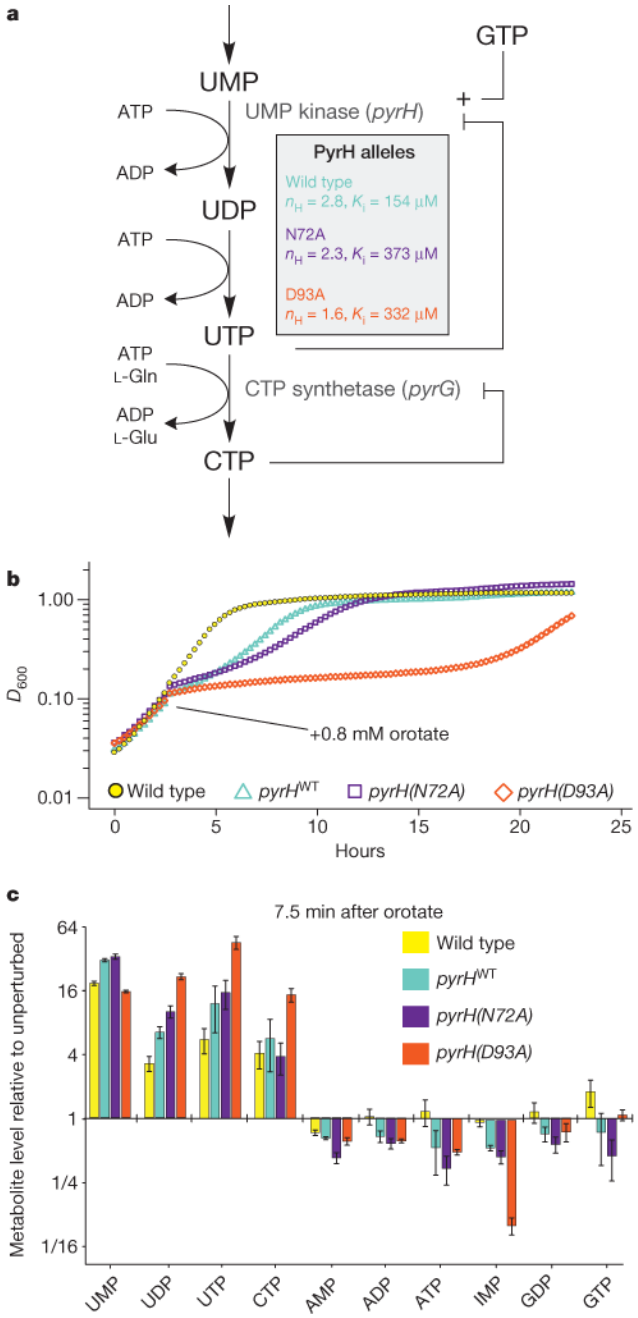

Figure 3. Cooperative inhibition of UMP kinase by UTP maintains end-product homeostasis

Variant *pyrH* alleles were expressed from its native promoter on low-copy plasmid (pACYC) with genomic *pyrH* removed. **a,** Schematic of downstream regulatory events in pyrimidine metabolism. Wild-type UMP kinase (PyrH) is feedback inhibited by UTP in a switch-like manner (high degree of cooperativity). Allosteric parameters of *pyrH* alleles appear in shaded box, with D93A lacking the switch-like behaviour. *n*H, Hill coefficient. **b,** Altered expression or regulation of UMP kinase following orotate addition impairs growth. Defects also occur in $pyrH^{WT}$/*pyrH* diploid strains (Supplementary Fig. 6). **c,** Metabolite fold changes upon orotate addition in strains with altered UMP kinase expression or

allosteric regulation reveal defects in both pyrimidine and purine homeostasis. Error bars mark standard deviation (n = 3).

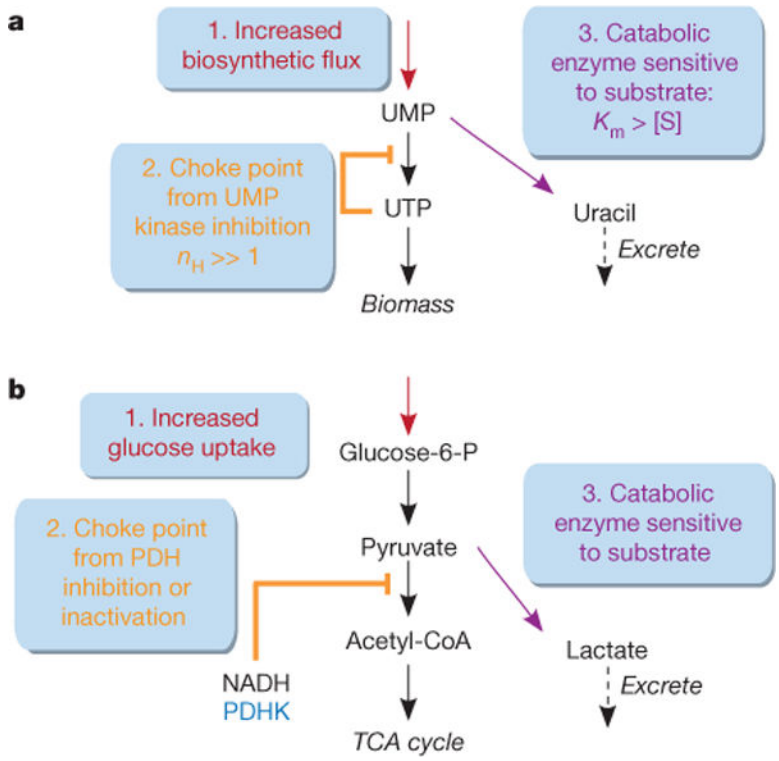

Figure 4. Directed overflow metabolism in biosynthesis is analogous to central carbon overflow metabolism

a, Schematic of directed overflow metabolism as a biosynthetic regulatory mechanism. **b,** Schematic of overflow in central carbon metabolism, using the Warburg effect as a canonical example. PDH, pyruvate dehydrogenase; PDHK, pyruvate dehydrogenase kinase (which catalyses inhibitory phosphorylation of PDH); TCA, tricarboxylic acid.